Stabilization of Metal-Rich Compounds by Polar-Intermetallic Bonding. Synthesis, Structure, and Bonding in Hf_5MTe_3 (M = Fe, Co)

Robert L. Abdon and Timothy Hughbanks*

Contribution from the Department of Chemistry, Texas A&M University, College Station, Texas 77843

Received June 14, 1995[⊗]

Abstract: The synthesis of the new ternary hafnium tellurides Hf_5MTe_3 (M = Fe, Co) and Hf_8MTe_6 (M = Co, Ni, Ru) is reported. The single-crystal structure of Hf_5FeTe_3 has been determined. Hf_5FeTe_3 crystallizes in the orthorhombic space group *Pnma* (No. 62) with lattice parameters a = 17.837(1) Å, b = 3.7044(5) Å, c = 13.183(2) Å (Z = 4); the lattice parameters for the Co analog show a slight shortening of all axes: a = 17.805(4) Å, b = 3.698(2) Å, c = 13.165(6) Å. The single-crystal structure of Hf_8FeTe_6 has also been determined. Hf_8FeTe_6 crystallizes in the orthorhombic space group *Pmmn* (No. 59) with lattice parameters a = 25.815(5) Å, b = 3.7309(7) Å, c = 7.598(1) Å (Z = 2); the lattice parameters for the new Co, Ni, and Ru analogs are reported. M-centered, tricapped, trigonal prisms of hafnium constitute the basic structural unit of both sets of compounds, and in both structure types these clusters condense to form one-dimensional chains. The more metal-rich composition of Hf_5MTe_3 is achieved through edge sharing of clusters within such chains to form double chains. Tellurium coordination is nearly identical in Hf_5FeTe_3 and Hf_8FeTe_6, producing strikingly similar channels that run parallel to the b axis. Four-probe resistivity measurements show metallic behavior for Hf_5FeTe_3, in accord with electronic structure calculations. These calculations also show that Hf−Fe bonding is of primary importance in stabilizing this structure type.

Introduction

More than 20 years ago, Brewer and Wengert predicted the trends in stability of transition metal alloys.[1] Very stable alloys were predicted for compounds formed by the combination of early- and late-d metals. A Lewis acid/Lewis base interaction was proposed whereby the paired d electrons of the late transition metal are donated to the empty, acceptor orbitals of the early transition metal. The most negative heats of formation are to be expected for alloys in which this interaction is optimized. This consideration, coupled with the increased importance of metal−metal bonding for 4d and 5d transition elements, led Brewer to predict the largest heats of formation for alloys of Hf and the group 8A metals. Topor and Kleppa have reported thermodynamic data for a number of binary intermetallics involving these elements.[2] Whatever the validity of the bonding picture proposed by Brewer, the thermodynamic stability of such intermetallic compounds is undeniable.

The stabilization conferred by this strong, polar-intermetallic bonding has only recently been exploited for the synthesis of new materials. Corbett and co-workers reported "alloy clusters" of zirconium and several rare-earth iodides.[3] In these compounds late transition metals (Mn to Ni) are encapsulated within octahedral clusters of the early metal. In Zr_6FeI_{14}, for example, the Fe atom occupies the center of a Zr_6 octahedron making bonds only to Zr—there are no Fe−I bonds. This chemistry has since been extended to include a number of zirconium and rare-earth halides which are stabilized by late-transition-metal interstitials.[4−12]

Parallel with these developments, Harbrecht and Franzen reported the synthesis of the $Ta_9M_2S_6$ (M = Fe, Co, Ni) series of compounds, in which condensed, tricapped, trigonal-prismatic, tantalum clusters are centered by a late transition element.[13] Tight-binding band structure calculations on the $Ta_9M_2S_6$ materials indicated that strong Ta−M bonding plays a key role in the stabilization of these unusual materials.[14] The related compounds $Ta_{11}M_2Se_8$ and Ta_8MSe_8 have since been reported and are built up from the same chains of M-centered, tantalum clusters.[15,16] Chains of condensed, M-centered, square antiprisms, $^1_\infty[Ta_4M]$, are found in Ta_4MTe_4 and Nb_4MTe_4 (M = Al, Si, Cr to Ni).[17,18] Single-crystal resistivity measurements show that these materials exhibit unusual resistivity anomalies and metal-insulator transitions consistent with charge-density wave formation.[19] Hoffmann and co-workers have performed extended Hückel calculations that again implicate strong

* Author to whom correspondence should be addressed.
[⊗] Abstract published in *Advance ACS Abstracts*, October 1, 1995.

(1) Brewer, L.; Wengart, P. R. *Metall. Trans.* **1973**, *4*, 83−104.
(2) Topor, L.; Kleppa, O. J. *J. Less-Common Met.* **1989**, *155*, 61−72.
(3) Hughbanks, T.; Rosenthal, G.; Corbett, J. D. *J. Am. Chem. Soc.* **1986**, *108*, 8289−8290.
(4) Hughbanks, T.; Rosenthal, G.; Corbett, J. D. *J. Am. Chem. Soc.* **1988**, *110*, 1511−1516.
(5) Hughbanks, T.; Corbett, J. D. *Inorg. Chem.* **1988**, *27*, 2022−2026.
(6) Kauzlarich, S. M.; Hughbanks, T.; Corbett, J. D.; Klavins, P.; Shelton, R. N. *Inorg. Chem.* **1988**, *27*, 1791−1797.
(7) Hughbanks, T.; Corbett, J. D. *Inorg. Chem.* **1989**, *28*, 631−635.
(8) Payne, M. W.; Dorhout, P. K.; Kim, S.-J.; Hughbanks, T. R.; Corbett, J. D. *Inorg. Chem.* **1992**, *31*, 1389−1394.
(9) Payne, M. W.; Dorhout, P. K.; Corbett, J. D. *Inorg. Chem.* **1991**, *30*, 1467−1472.
(10) Dorhout, P. K.; Corbett, J. D. *J. Am. Chem. Soc.* **1992**, *114*, 1697−1701.
(11) Dorhout, P. K.; Payne, M. W.; Corbett, J. D. *Inorg. Chem.* **1991**, *30*, 4960−4962.
(12) Ruck, M.; Simon, A. *Z. Anorg. Allg. Chem.* **1993**, *619*, 327−336.
(13) Harbrecht, B.; Franzen, H. F. *J. Less-Common Met.* **1985**, *113*, 349−360.
(14) Calhorda, M. J.; Hoffmann, R. *Inorg. Chem.* **1988**, *27*, 4679−4686.
(15) Harbrecht, B. *J. Less-Common Met.* **1988**, *141*, 59−71.
(16) Conrad, M.; Harbrecht, B. *J. Alloys Comp.* **1993**, *197*, 57−64.
(17) Badding, M. E.; DiSalvo, F. J. *Inorg. Chem.* **1990**, *29*, 3952−3954.
(18) Neuhausen, J.; Finckh, E. N.; Tremel, W. *Chem. Ber.* **1995**, *128*, 569−573.

0002-7863/95/1517-10035$09.00/0

Ta(Nb)−M bonding in the stabilization of this unique structure.[20] In many of these materials, chalcogens serve to "decorate" the metal−metal bonded framework producing materials with highly anisotropic properties.

Recent investigations of group V tellurides have further demonstrated the importance of strong intermetallic bonding. In $Nb_2Co_2Te_4$, TaM_2Te_2 (M = Co, Ni),[21] and $NbMTe_2$ (M = Fe, Co)[22] one finds metal−metal bonded layers featuring bonds between early and late transition metals. Tellurium constitutes the exterior of the layers, and layers are held together by weak van der Waals interactions. Calculations on $TaCo_2Te_2$ show that the structure is stabilized by strong Ta−Co interactions,[23] in accord with Brewer's ideas.

We have uncovered new and interesting chemistry in our studies of hafnium−telluride binary and ternary systems. We recently reported Hf_3Te_2, a layered material formally related to body-centered-cubic hafnium.[24] Two pseudo-binary materials stabilized by zirconium have also been characterized. $Hf_{(3-x)}Zr_xTe_4$ (Nb_3Te_4-type) is built up from face- and edge-sharing MTe_6 octahedra which produce large trigonal antiprismatic channels within the structure.[25] $Hf_{(5-x)}Zr_xTe_4$ adopts an undistorted Ti_5Te_4-type structure.[26] The ternary compounds Hf_8MTe_6 (M = Mn, Fe)[27] possess structural features quite similar to those exhibited by the $Ta_9M_2S_6$ compounds discussed above and were the first ternary hafnium chalcogenides to exhibit strong polar-intermetallic bonding.

In this paper we report the synthesis, structure, and electrical property measurements of the new ternary tellurides Hf_5MTe_3 (M = Fe, Co). A structural comparison of these new compounds with the previously reported Hf_8MTe_6 materials and new results concerning the latter compounds are also presented. The results of band structure calculations serve to aid in the analysis of structural features and electronic properties.

Experimental Procedures

Syntheses. The elemental powders, Hf (99.6% including 1.29 wt % Zr, Teledyne Wah Chang), Te (99.99%, Johnson Matthey), Fe (99.99+%, Aldrich), Co (99.8%, Aesar), Ni (99.996%, Johnson Matthey), and Ru (99.95%, Johnson Matthey), were used as starting materials. Elemental mixtures were sealed in Nb capsules that were in turn sealed in evacuated (~10^{-4} Torr) silica ampules. Hf_5FeTe_3 was first obtained as a minor product in the preparation of Hf_8FeTe_6. Subsequent reactions which were heated slowly to 1000 °C and held at this temperature for 1−2 weeks suggested the new compound's more metal-rich composition. Guinier powder films from these reactions show that Hf_5FeTe_3 remains contaminated by a small amount of Hf_8FeTe_6. A sample loaded at the composition Hf_4FeTe_2 was first heated to 900 °C over 8 days and held at this temperature for 4 days. The reaction was cooled to 400 °C over 4 days and then quenched to room temperature. The resulting powder was cold-pressed into a pellet and melted (~50 a, 50 V) twice for 30 s on an oxygen-free copper hearth under an argon atmosphere. A 3.8% mass loss due to tellurium volatilization during the melting process was determined by difference. The Guinier powder diffraction pattern of this material showed only Hf_5FeTe_3. Polished fragments from this reaction were analyzed by wavelength dispersive spectrometry and yielded the approximate composition $Hf_{10.59}Fe_2Te_{6.43}$. No impurity elements other than Zr (less than 0.6 wt %) were detected. Attempts to prepare this material in sealed Nb ampules at the analyzed composition produced Hf_8FeTe_6 as the major phase. Subsequent arc-melting of these reaction products also showed primarily Hf_8FeTe_6; however, a small amount of the desired phase was also detected in the Guinier powder diffraction pattern.

Table 1. Lattice Parameters (Å) of Hf_5MTe_3 Phases (Space Group *Pnma*)[a]

	Hf_5FeTe_3	Hf_5CoTe_3
a	17.837(1)	17.805(4)
b	3.7044(5)	3.698(2)
c	13.183(2)	13.165(6)

[a] Refined from Guinier powder diffraction patterns using Si as an internal standard.

Crystals of suitable size for X-ray diffraction experiments were obtained from a reaction mixture slightly rich in both hafnium and iron. A total of 0.5 g of the elements in the molar ratio Hf:Fe:Te = 9:2:5 was heated rapidly to 500 °C then ramped to 950 °C over 6 days. The reaction was held at this temperature for 2 days before increasing the temperature to 1000 °C over a 3-day period. The reaction was allowed to proceed at this temperature for 12 days before quenching to room temperature. The microcrystalline product was cold-pressed into a pellet and melted twice in the manner described above (32 a, 50 V). The resulting ingot contained large needle-like formations aligned in the direction from which the arc had been applied. Mass loss due to tellurium volatilization during melting was 2.6%. The Guinier diffraction pattern of the sample prepared in this manner showed only the new Hf_5FeTe_3 phase.

After the structure and composition had been determined, a powder sample of Hf_5FeTe_3 was obtained in quantitative yield by first heating a stoichiometric mixture of the elements at 1000 °C for 10 days then melting under Ar as described above. The powder diffraction pattern of this sample matched the pattern calculated from the crystal structure. The Co-containing compound is obtained using an exactly analogous procedure.

Preparation of Hf_8FeTe_6 has been previously reported.[27] The isostructural Co, Ni, and Ru compounds are made following the procedure described for Hf_8FeTe_6 followed by arc-melting as described above. Typical mass loss during melting is ~2%. Guinier powder patterns show only the Hf_8MTe_6 structure type for the Co- and Ni-containing materials when prepared in this manner. The Ru-containing material shows significant amounts of Hf_3Te_2 and the binary alloy HfRu even after repeated melting. Annealing of crushed arc-melted ingots at 1000 °C results in decomposition of these new ternary Hf_8MTe_6 compounds to binary hafnium tellurides and Hf−M intermetallics.

X-ray Studies. (a) Hf_5FeTe_3. A black, blade-shaped crystal having approximate dimensions of 0.01 × 0.31 × 0.03 mm^3 was selected from a crushed, arc-melted ingot and mounted in a 0.2 mm diameter glass capillary. Preliminary indexing of the Guinier powder diffraction data established the orthorhombic unit cell and lattice constants. All measurements were made on a Siemens R3m/V diffractometer with graphite-monochromated Mo Kα radiation at room temperature. Cell constants matching those from the Guinier data and an orientation matrix were obtained from a least-squares refinement using data from 10 centered reflections. This cell was further refined by centering on 19 reflections in the range $15° < 2\theta < 30°$. The cell parameters (refined from Guinier powder diffraction patterns) for both the Fe- and the Co-containing compounds are given in Table 1. Data were collected using $\theta-2\theta$ scans for reflections with $2\theta < 50°$. Three check reflections were monitored periodically and showed no significant changes during the 2-day data collection process. Two octants of data were collected ($+h,+k,\pm l$) to gain the advantage of averaging. Systematic absences reduced the possible space groups to $Pnm2_1$ (No. 31) and *Pnma* (No. 62). The Hf and Te atoms were located by direct methods in the centrosymmetric space group *Pnma*. The partial structure was refined isotropically against F^2 using SHELX93.[28] The Fe atom was located inside the cluster as the largest residual in the

(19) Ahn, K.; Hughbanks, T.; Rathnayaka, K. D. D.; Naugle, D. G. *Chem. Mater.* **1994**, *6*, 418−423.
(20) Li, J.; Hoffmann, R.; Badding, M. E.; DiSalvo, F. J. *Inorg. Chem.* **1990**, *29*, 3943−3952.
(21) Tremel, W. *Angew. Chem., Int. Ed. Engl.* **1992**, *31*, 217−220.
(22) Li, J.; Badding, M. E.; DiSalvo, F. J. *Inorg. Chem.* **1992**, *31*, 1050−1054.
(23) Tremel, W. *J. Chem. Soc., Chem. Commun.* **1991**, 1405−1407.
(24) Abdon, R. L.; Hughbanks, T. *Angew. Chem., Int. Ed. Engl.* **1994**, *33*, 2328−2330.
(25) Wang, C. C.; Abdon, R. L.; Hughbanks, T.; Reibenspies, J. *J. Alloys Comp.* In Press.
(26) Abdon, R. L.; Ahn, K.; Hughbanks, T. Unpublished research.
(27) Abdon, R. L.; Hughbanks, T. *Chem. Mater.* **1994**, *6*, 424−428.
(28) Sheldrick, G. M. In *Nicolet Analtyical X-ray Instruments*: Göttingen, Germany, 1993.

Table 2. Lattice Parameters (Å) of Hf_8MTe_6 Phases (Space Group *Pmmn*)[a]

	Hf_8MnTe_6	Hf_8FeTe_6	Hf_8CoTe_6	Hf_8NiTe_6	Hf_8RuTe_6
a	25.816(4)	25.815(5)	25.709(2)	25.65(1)	25.80(1)
b	3.7614(6)	3.7309(7)	3.7373(6)	3.749(1)	3.761(2)
c	7.605(2)	7.598(1)	7.625(1)	7.602(3)	7.600(7)

[a] Refined from Guinier powder diffraction patterns using Si as an internal standard.

Table 3. Crystallographic Data for Hf_5FeTe_3 and Hf_8FeTe_6

	Hf_5FeTe_3	Hf_8FeTe_6
chemical formula	Hf_5FeTe_3	Hf_8FeTe_6
V, Å^3	871.1(2)	731.8(5)
Z	4	2
formula wt	1331.10	2249.37
space group	*Pnma* (No. 62)	*Pmmn* (No. 59)
T, °C	23	−110
λ, Å	0.71073	0.71073
abs coeff (μ), mm^{-1} (Mo Kα)	70.704	69.105
crystal dimens, mm	0.01 × 0.31 × 0.03	0.01 × 0.25 × 0.01
2θ(max), deg	50	50
no. of reflcns		
measured	1536 (h,±k,l)	3105 (±h,±k,l)
unique	897 (R_{int} = 5.98%)	773 (R_{int} = 12.49%)
unique obsd ($F_o^2 > 2\rho(F_o^2)$)	444	602
no. of variables	56	50
secondary ext. coeff (×10^{-4})		1.8
$R1$;[a] $wR2$,[b] % ($I > 2\rho(I)$)	3.27; 5.26	3.60; 7.02
$R1$;[a] $wR2$,[b] % (all data)	9.96; 6.70	6.10; 7.97
goodness of fit indicator	1.031	1.088
max (min) peaks in the final diff map, e$^-$/Å^3	2.659 (−3.418)	3.225 (−3.303)

[a] $R1(F) = \sum(||F_o| - |F_c||)/\sum|F_o|$. [b] $wR2(F^2) = \{\sum[w(F_o^2 - F_c^2)^2]/\sum[w(F_o^2)^2]\}^{1/2}$, $w = \exp[c(\sin(\theta/\lambda))^2]/[\rho^2(F_o^2) + (xP)^2 + yP]$, $P = (F_o^2 + 2F_c^2)/3$ (Hf_5FeTe_3: $x = 0.0058$, $y = 0.0$, $c = 5.0$; Hf_8FeTe_6: $x = 0.0166$, $y = 19.1745$, $c = 0$).

difference map. Correction of the data by the Ψ-scan method based on four reflections (only four had χ angles near 90° with suitable intensity) and subsequent refinement of the structure resulted in improved R values; however, an additional absorption problem was evident when anisotropic refinement produced thermal ellipsoids all following the trend $U_{11} > U_{22} > U_{33}$. After correcting the data with DIFABS,[29] anisotropic refinement resulted in reasonably isotropic thermal ellipsoids for all atoms except Fe ($U_{22} = 3U_{11}$, $U_{33} = 2U_{11}$). However, DIFABS also increased the magnitude of some otherwise weakly negative reflections and residuals for the full (adjusted) data set were thereby increased. While this motion may represent a genuine physical phenomenon, it is more likely the result of disorder associated with higher defect concentrations in these rapidly quenched samples. Similar peculiarities in thermal parameters have been observed for structurally related materials. The structure was refined to final values for *R1* and *wR2* of 3.27 and 5.28%, respectively. The largest remaining peaks in the final Fourier difference map were 2.659 and −3.390 e$^-$/Å^3 located 1.49 Å from Te3 and 1.40 Å from Hf2, respectively. A summary of crystal and data collection parameters may be found in Table 3.

(b) Hf_8FeTe_6. A black, needle-shaped fragment having dimensions 0.01 × 0.25 × 0.01 mm^3 was selected from a crushed, arc-melted ingot of Hf_8FeTe_6 and mounted on a glass fiber. All measurements were performed on a Rigaku AFC5R diffractometer equipped with a 12-kW rotating anode generator with graphite monochromated Mo Kα radiation at −110 °C. Cell constants and an orientation matrix were obtained from a least-squares refinement using 25 centered reflections in the range $39 < 2\theta < 49°$. Data were collected by ω scans for reflections with $2\theta < 50°$. Three check reflections were monitored periodically and showed no significant trend during the 38-h data collection process. A hemisphere of data was collected (±h,±k,+l) to gain the advantage of averaging. The data were corrected for absorption using the Ψ-scan technique based on three reflections. As

(29) Walker, N.; Stuart, D. *Acta Crystallogr.* **1983**, *A39*, 158−166.

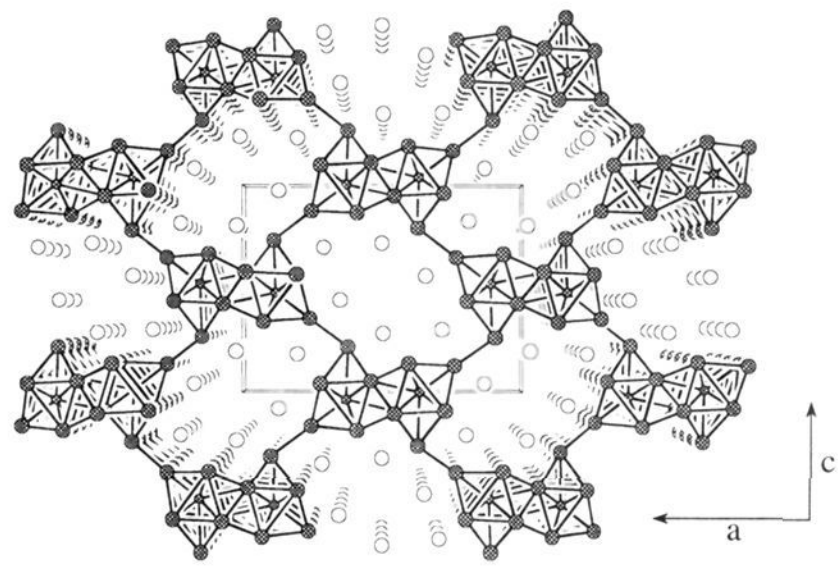

Figure 1. (010) projection of the Hf_5FeTe_3 structure. Hf atoms are shown as the hatched circles, Fe as the small hatched circles, and Te as the large open circles. Bonds shown indicate the Hf−Hf and Hf−Fe contacts.

expected, reflection conditions and intensity statistics suggested the space group *Pmmn* (No. 59). The structure was refined against F^2 using SHELX93. The atomic coordinates for Hf_8MnTe_6 were used as a trial structure. Isotropic refinement proceeded without incident for this known structure type. Anisotropic refinement of the atomic parameters resulted in elongated thermal ellipsoids directed along the needle axis. DIFABS was used to correct the data for this additional absorption problem and resulted in generally isotropic ellipsoids for all atoms except Fe ($U_{11} = 4U_{22}$, $U_{33} = 7U_{22}$). Statistical analysis of the data suggested the need for a secondary extinction coefficient which refined to a value of 1.8×10^{-4}. The structure refined to a final residual of 3.60% and 7.02% for R and R_w, respectively. The largest remaining peaks in the final Fourier difference map were 3.225 and −3.303 e$^-$/Å^3 located in the framework of the structure. A summary of crystal and data collection parameters may be found in Table 3. The cell parameters for Hf_8MTe_6 compounds, obtained from refinement of Guinier powder diffraction data, are given in Table 2.

Electrical Resistivity Measurements. Since Hf_5FeTe_3 is sensitive to air and moisture, all resistivity measurements were carried out in an inert atmosphere. The single-crystal resistivity measurements were made using the dc four-probe method. Four contacts were made with silver epoxy (Acme E-solder 3021) and leads from the contacts were made with 0.05 mm diameter gold wires. All measurements were repeated at least twice on separate crystals. Resistivities were measured with cooling and warming over the range 77−300 K and showed no thermal hysteresis, indicating good temperature equilibration throughout the measurement.

Results and Discussion

The structure of Hf_5FeTe_3 exhibits a novel metal−metal bonded framework of condensed, tricapped, trigonal-prismatic, hafnium clusters. In the center of each cluster sits an iron atom. The tellurium atoms serve to line this framework producing large channels parallel to the Hf clusters. The structure is shown in Figure 1 projected onto the *a*,*c* plane. For clarity only the metal−metal bonded framework is shown.

The clusters in Hf_5FeTe_3 are built up from eclipsed, Hf_3 triangles to form columns of trigonal prisms running along the *b* axis of the crystal. Another hafnium atom caps each square face of these prisms to form a tricapped, trigonal prismatic chain. Individual chains are condensed along an edge such that one capping hafnium and one inner hafnium are shared by two clusters to form double chains. One such column is depicted in Figure 2. The unit cell contains two such chains. Each of the four capping hafnium atoms of the double chain that are not involved in condensation make two longer bonds to capping atoms of a neighbor chain, stitching the chains together into a three-dimensional network.

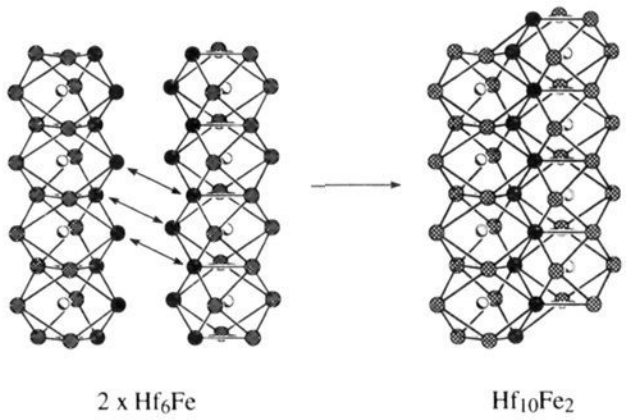

Figure 2. Individual Hf_6Fe cluster chains condense through edge sharing to produce double chains in the Hf_5FeTe_3 structure. Large circles are Hf, small circles are Fe. Darkened Hf atoms depict those that are shared in the double chains. For clarity only Hf−Hf bonds are shown.

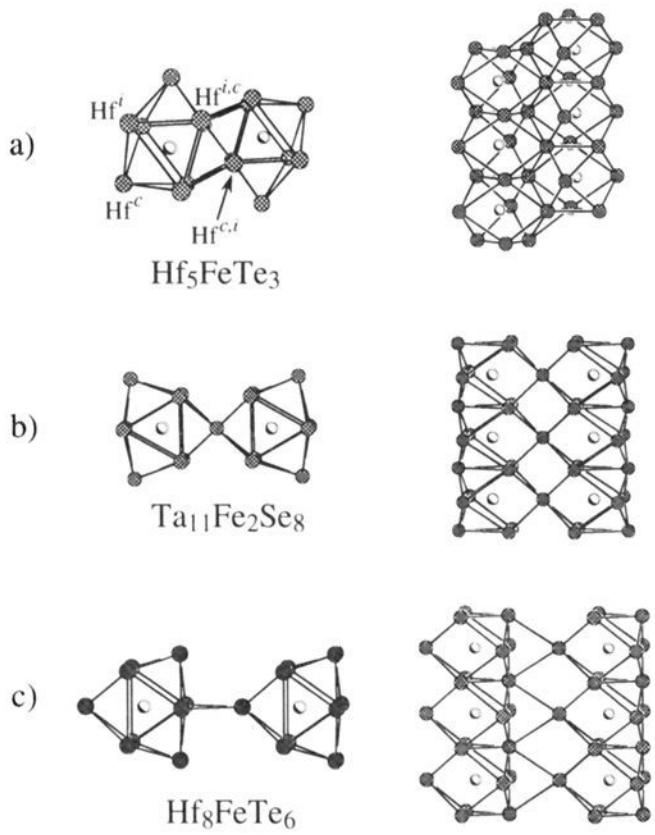

Figure 3. Top and side views of (a) edge-sharing double chains in Hf_5FeTe_3, (b) vertex-sharing columns in $Ta_{11}Fe_2Se_8$, and (c) linkage of complete Hf_6Fe clusters in Hf_8FeTe_6. Hf and Ta atoms are the larger cross-hatched circles, Fe atoms are the smaller circles.

The linked, double chains within the Hf_5FeTe_3 structure represent a new type of tetrakaidecahedral cluster network. Figure 3 shows top and side views of condensed clusters in Hf_5FeTe_3, $Ta_{11}Fe_2Se_8$, and Hf_8FeTe_6 materials. Edge sharing of the tricapped trigonal prismatic clusters in Hf_5FeTe_3 results in alternating heights of the clusters along the chain axis. Adjacent columns are displaced along by 1/2*b* with respect to any individual double chain (Figure 3a). Double chains in $Ta_{11}Fe_2Se_8$ are also displaced with respect to neighbor chains; however, fusion through one capping atom produces double chains where cluster heights do not alternate (Figure 3b). The Hf_8FeTe_6 structure contains complete, uncondensed Hf_6Fe clusters linked by bonds between a hafnium atom of each inner trigonal prism and a capping hafnium of a neighboring chain's cluster (Figure 3c), producing layers in which all clusters sit at the same height. The $Nb_8M_2S_4$ structure reported by Harbrecht results from edge-shared, double chains, like those found in Hf_5FeTe_3, which further condense through sharing of the remaining capping atoms as described for $Ta_{11}Fe_2Se_8$.[30]

While the linkage of tetrakaidecahedral clusters is quite different in the Hf_8FeTe_6 and Hf_5FeTe_3 structures (see Figure 4), the clusters themselves are similarly shaped. Distances

(30) Harbrecht, B. Habilitation Thesis, Universität Dortmund, 1989.

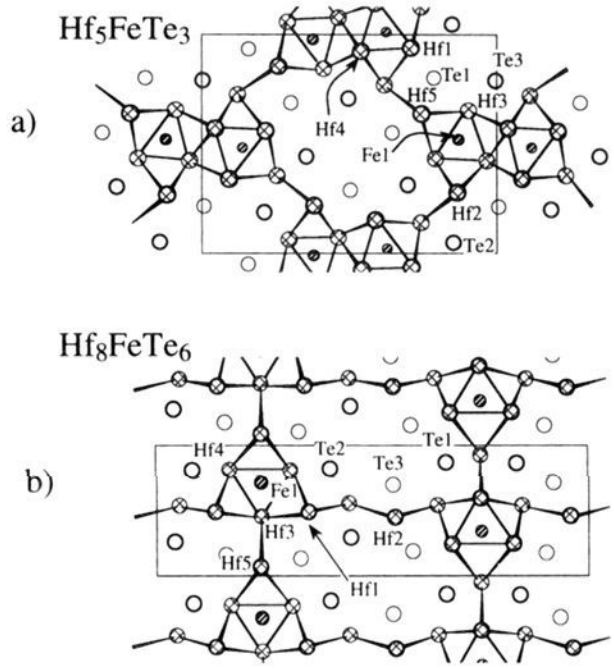

Figure 4. (010) projections of the Hf_5FeTe_3 (a) and Hf_8FeTe_6 (b) structure types. Cross-hatched circles are Hf, hatched circles are Fe, and open circles are Te. The atom labeling scheme corresponds to atom designations in Table 4. For clarity only Hf−Hf bonds are depicted.

within the M-centered clusters of Hf_8FeTe_6 and Hf_5FeTe_3 are compared in **1**. In the Hf_8MTe_6 structure, the Hf_6 trigonal prisms

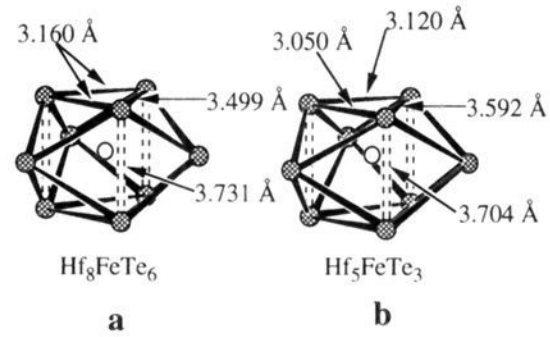

1

of the cluster core are shaped such that the triangular faces are isosceles ($d_{Hf-Hf} = 1 \times 3.499, 2 \times 3.160$ Å). The inner trigonal prisms of Hf_5FeTe_3 are also distorted to form one longer and two shorter bonds, 3.592, 3.120, and 3.050 Å, respectively. In both structures the Hf_3 triangles are widely separated (3.731 Å in Hf_8FeTe_6 and 3.704 Å in Hf_5FeTe_3); this separation is just the *b* axis length and is set by the steric demands of the tellurium atoms.

The geometric similarity between the hafnium clusters in the Hf_8FeTe_6 and Hf_5FeTe_3 structure types enforces similar coordination environments for the centering elements as well. In both structures the iron atom moves away from the center into the elongated, square face of the trigonal prism. In Hf_5FeTe_3 this results in the formation of four shorter bonds (2×2.617, 2×2.656 Å) to the Hf1 and Hf3 atoms of the trigonal prism and a bond of comparable length (1×2.807 Å) to Hf5 which caps the elongated, prism face. Pairing of the 3d metals has been reported for $Ta_9M_2S_6$ (M = Fe, Co) and is suspected in the $Ta_{11}M_2Se_8$ structure as well;[15,31] however, we find no evidence for such a distortion in Hf_5FeTe_3. Important bond distances for Hf_5FeTe_3 are gathered in Table 4.

As in the Hf_8FeTe_6 structure, the tellurium atoms in Hf_5FeTe_3 are 4-, 5-, and 6-coordinate producing strikingly similar tellurium-lined channels that run parallel to the short axis of the structure. Interatomic distances for these channels in the two structures are compared in **2**. Lines connecting Te atoms are not meant to indicate bonding interactions, but rather to guide the eye. This view suggests that the most likely place for the

(31) Harbrecht, B. *J. Less-Common Met.* **1986**, *124*, 125−134.

Table 4. Important Interatomic Distances (Å) for Hf_5FeTe_3[a,b]

Hf^i–Hf^i		Fe–Hf^c	
Hf1–Hf3 (1×)	3.591(3)	Fe1–Hf2	3.108(4)
		Fe1–Hf5	2.807(6)
Hf^i–$Hf^{i,c}$			
Hf1–Hf4 (1×)	3.050(3)	Fe–$Hf^{c,i}$	
Hf3–Hf4 (1×)	3.120(3)	Fe1–Hf4a (1×)	3.071(7)
Hf^i–Hf^c		6-coordinate Te	
Hf1–Hf2 (2×)	3.288(2)	Te1–Hf1 (2×)	2.940(3)
Hf1–Hf5 (2×)	3.313(2)	Te1–Hf3 (1×)	2.885(4)
Hf3–Hf5 (2×)	3.357(2)	Te1–Hf5 (2×)	2.934(3)
		Te1–Hf2 (1×)	3.113(4)
Hf^i–$Hf^{c,i}$			
Hf3–Hf4a (2×)	3.164(2)	5-coordinate Te	
		Te3–Hf2 (2×)	2.998(3)
$Hf^{i,c}$–Hf^c		Te3–Hf3 (2×)	3.005(3)
Hf4–Hf2 (2×)	3.102(2)	Te3–Hf4 (1×)	2.987(2)
Fe–Hf^i		4-coordinate Te	
Fe1–Hf1 (2×)	2.617(5)	Te2–Hf1 (1×)	2.940(3)
Fe1–Hf3 (2×)	2.656(5)	Te2–Hf2 (1×)	2.917(4)
		Te2–Hf5 (2×)	2.892(3)
Fe–$Hf^{i,c}$			
Fe1–Hf4 (2×)	2.700(5)		

[a] Hf^i: Hf atom of inner trigonal prism. Hf^c: Hf atom capping the trigonal prism. $Hf^{i,c}$: Hf atom of an inner trigonal prism which is capping with respect to neighbor cluster. $Hf^{c,i}$: Hf atom capping the trigonal prism that also forms the inner trigonal prism of the neighbor cluster (see Figure 3a). [b] Distances were calculated using cell parameters reported in Table 1.

potential incorporation of cations is in the interstice formed by the Te2 and Te3 atoms. The distorted, monocapped, trigonal-prismatic coordination environment of this site is the most regular and is large enough for small ions such as Li^+. The presence of these channels in both structures might suggest a certain stability associated with this arrangement; however, the presence of channels with different chalcogen arrangements in the related Ta-containing materials and the overriding importance of polar-intermetallic bonding suggest that hafnium telluride materials with a variety of structures may still be prepared.

It is clear from the details surrounding the preparation of Hf_5FeTe_3 and Hf_5CoTe_3 that both these compounds are stable over wide temperature ranges. Reactions designed to prepare the Fe-containing compound that were quenched after remaining at 1000 °C for 2–4 weeks show a mixture of Hf_5FeTe_3 and Hf_8FeTe_6, while under the same conditions only binary hafnium tellurides are observed in reactions intended to yield Hf_5CoTe_3.

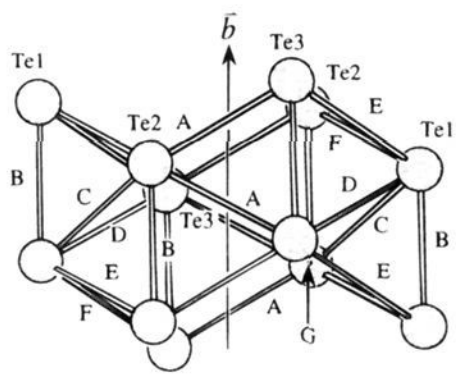

	Hf_8FeTe_6	Hf_5FeTe_3
A	4.137 Å	3.822 Å
B	3.731	3.704
C	3.749	4.088
D	3.745	3.909
E	3.768	4.088
F	3.764	3.909
G	3.798	4.345

Table 5. Parameters for EH Calculations

	orbital	H_{ii}, eV	ζ_1[b]	ζ_2[b]	c_1[a]	c_2[a]
Hf	5d	−8.17	4.36	1.709	0.6967	0.5322
	6s	−8.17	2.21			
	6p	−4.57	2.17			
Fe	3d	−9.35	5.55	1.800	0.5411	0.6734
	4s	−7.73	1.90			
	4p	−3.86	1.90			
Te	5s	−21.20	2.51			
	5p	−12.00	2.16			

[a] Coefficients used in double-ζ expansion. [b] Slater-type orbital exponents.

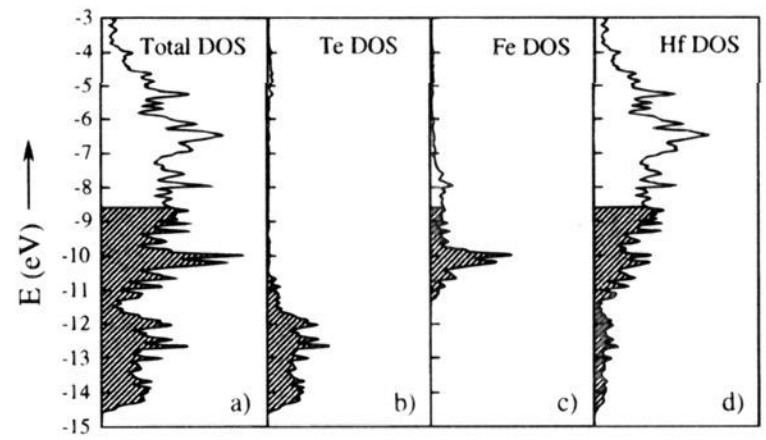

Figure 5. (a) Total density of states (DOS) diagram for Hf_5FeTe_3. The energy range includes the Te 5p bands and the transition metal d and s bands. (b) Tellurium contribution to the DOS. (c) Fe contribution to the DOS. (d) Hf contribution to the DOS. Filled levels are shaded.

However, when either compound is prepared in an arc-melting reaction, they are stable indefinitely when maintained at temperatures at or below 1000 °C. High temperatures are necessary to overcome kinetic barriers to these compounds' formation, but once formed they are stable. In attempts to prepare Hf_5FeTe_3 at 1000 °C, Hf_8FeTe_6 forms first and is only slowly converted to Hf_5FeTe_3. For the Co-containing compound, the presence of binary hafnium tellurides at 1000 °C suggests that elemental Co remains inert in this system.

The importance of Te–Te bonding in transition metal ditellurides is well documented.[32] In compounds containing later transition metals in high formal oxidation states, the overlap of the metal d manifold and the Te 5p bands results in Te oxidation and consequent Te–Te bond formation. However, in metal-rich compounds of the early transition metals fully reduced Te can be expected. In these materials, early transition metals in low oxidation states have d bands which lie well above the Te 5p bands and the latter bands remain entirely filled. No "internal oxidation–reduction" occurs. In Hf_5FeTe_3, the shortest Te–Te distance is determined by the *b* axis dimension, 3.704 Å. While this is shorter than the van der Waals distance of 4.0 Å, this separation represents a balance between the drive toward shorter Hf–Hf bonds and the avoidance of nonbonded Te–Te repulsions.

The electronic band structure of Hf_5FeTe_3 was calculated using the extended Hückel method, parameters for which are given in Table 5. The total density of states (DOS) diagram (Figure 5) shows that the material should be a metallic conductor, as would be intuitively expected for a structure containing a metal–metal bonded framework. The projected DOS in Figure 5b shows that the levels in the energy regime below −10.5 eV are primarily Te based. The projected DOS in panel c of Figure 5 shows that the levels with Fe character are confined to the range between −11.3 and −6.0 eV while the projection in panel d of Figure 5 shows that levels at higher

(32) Canadell, E.; Jobic, S.; Brec, R.; Rouxel, J.; Whangbo, M. H. *J. Solid State Chem.* **1992**, *99*, 189–199.

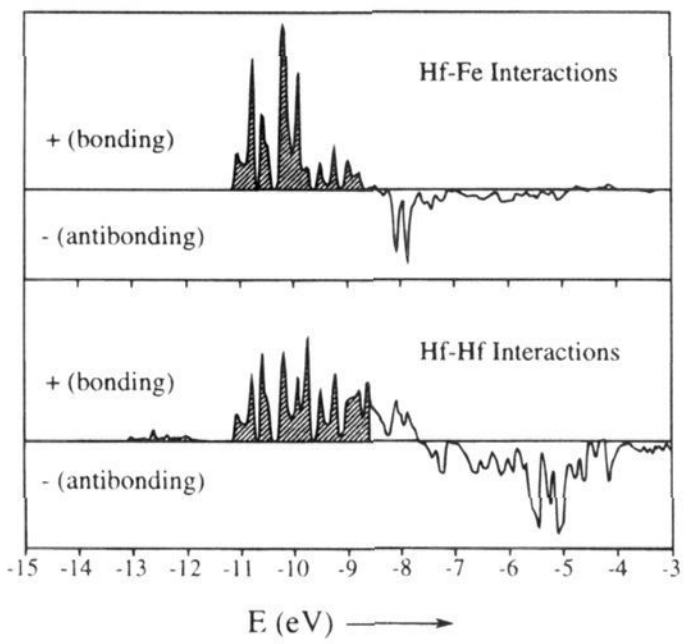

Figure 6. Averaged crystal orbital overlap population (COOP) curves for Hf−Fe and Hf−Hf contacts less than 3.2 and 3.6 Å, respectively. Levels above the horizontal axis are bonding while those below are antibonding. Filled levels are shaded. Note optimization of the Hf−Fe interactions in Hf_5FeTe_3.

energies have mainly Hf d and s character. This projection also shows significant mixing of hafnium character in the tellurium-based manifold indicating significant covalency in these materials.

The spatial segregation of the atoms within the Hf_5FeTe_3 structure is also manifest in the electronic structure. The Fe contribution to the DOS is restricted to the energy range between −11.3 and −6.0 eV. Despite the smaller energy separation between Fe 3d orbitals and Te p orbitals, the levels with Fe character are almost entirely excluded from the Te-based manifold. The DOS projections show that interactions are divided into primarily Hf−Te and Hf−Fe interactions. There are no close Fe−Te contacts—the electronic structure naturally reflects the absence of Fe−Te bonds.

Crystal orbital overlap populations (COOPs) were also calculated for the metal−metal bonded framework of Hf_5FeTe_3.[33] Figure 6 shows averaged curves for Hf−Fe and Hf−Hf interactions in the Hf_5FeTe_3 structure. The presence of significant Hf−Hf bonding character in levels above the Fermi level indicate Hf−Hf bonding would increase at higher electron concentrations. However, this figure also shows that Hf−Fe bonding is optimized; if the electron concentration were much higher or lower, Hf−Fe bonding would be weaker. As was the case in the Hf_8MTe_6 structure, it is the optimization of Hf−M bonding which seems to stabilize this unique metal−metal bonded framework.

In a more philisophical vein, we can ask whether the Brewer−Wengert Lewis acid/Lewis base bonding description is consistent with our treatment. Our results indicate that Hf−Fe bonding is polar covalent; Hf−Fe bonding levels are completely filled and primarily Fe localized while antibonding levels are vacant and primarily Hf localized. This is quite consistent with a Lewis acid/Lewis base (Hf/Fe) interaction. If one wishes to make the *nature of the bonds* between the early- and late-transition metals the central criterion for adopting the Lewis acid/Lewis base description, then we believe the Brewer−Wengert view to be generally valid. Our personal preference is to reserve the Lewis acid−base "label" for those instances where individual Lewis acids and Lewis bases are isolable species with structures that are clearly related to structures they assume after formation of a given Lewis acid−base pair. In other words, we feel that the Lewis description is most useful where it gives insight into reactivity as it relates to both what compounds will form *and* what structure they will adopt. With this more stringent requirement, the Brewer−Wengert analogy falls short—and no other simple theoretical concepts have been developed to fill the void which remains.

The electrical resistivity of Hf_5FeTe_3 shows a positive temperature coefficient indicative of simple metallic conductivity in the range 77−300 K. Crystals of this material all display high residual resistivity when extrapolated to $T = 0$ K. We believe that this is indicative of a high defect concentration. The presence of trace amounts of zirconium produces many defect sites within the lattice despite the tendency of hafnium-rich materials to fractionate to reduce zirconium content. There is also undoubtedly some disorder associated with rapid quenching from the melt. Both factors should reduce the electrons' mean free path. Zirconium-free starting materials and extended annealing times would be required to eliminate the residual resistivity.

Acknowledgment. This research was generously supported by the National Science Foundation through Grant No. DMR-9215890 and by the Robert A. Welch Foundation through Grant No. A-1132. We thank Yunchao Tian for help in performing band structure calculations and Kyungsoo Ahn for assistance with the resistivity measurements. The R3m/v single-crystal X-ray diffractometeer and crystallographic computing system were purchased from funds provided by the National Science Foundation (CHE-8513273). We thank Dr. Abraham Clearfield for the generous use of his facilities and Joseph Reibenspies for data collection on the Hf_8FeTe_6 material. We also thank Dr. Renald Guillemette for his assistance with the microprobe analyses and Teledyne Wah Chang for a gift of Hf powder.

Appendix

The extended Hückel method[34,35] was used for all band structure calculations; parameters appear in Table 5. Valence-state ionization energies (H_{ii}'s) for Hf and Fe were previously obtained from a charge-iterative calculation on Hf_8FeTe_6. Orbital exponents for Te were taken from Clementi and Roetti.[36] Band structure calculations were carried out using a 256*k* point mesh for the 3-D orthorhombic cell. DOS curves were smoothed with Gaussian functions with a half-width of 0.025 eV.

Supporting Information Available: Tables of crystal and refinement data and of anisotropic displacement parameters for Hf_5FeTe_3 and Hf_8FeTe_6 (3 pages). This material is contained in many libraries on microfiche, immediately follows this article in the microfilm version of the journal, can be ordered from the ACS, and can be downloaded from the Internet; see any current masthead page for ordering information and Internet access instructions.

JA9519445

(33) Hughbanks, T.; Hoffmann, R. *J. Am. Chem. Soc.* **1983**, *105*, 3528−3537.

(34) Hoffmann, R. *J. Chem. Phys.* **1963**, *39*, 1397−1398.

(35) Whangbo, M.-H.; Hoffmann, R. *J. Am. Chem. Soc.* **1978**, *100*, 6093−6098.

(36) Clementi, E.; Roetti, C. *At. Nucl. Data Tables* **1974**, *14*, 455.